

Consistency between domain wall oscillation modes and spin wave modes in nanostrips

Xinwei Dong(董新伟) and Zhenjiang Wu(吴振江)

Citation: Chin. Phys. B, 2024, 33 (**6**): 067502. DOI: 10.1088/1674-1056/ad2a6b
Journal homepage: http://cpb.iphy.ac.cn; http://iopscience.iop.org/cpb

What follows is a list of articles you may be interested in

Creation and annihilation of artificial magnetic skyrmions with the electric field

Jun Cheng(程军), Liang Sun(孙亮), Yike Zhang(张一可), Tongzhou Ji(吉同舟), Rongxing Cao(曹荣幸), Bingfeng Miao(缪冰锋), Yonggang Zhao(赵永刚), and Haifeng Ding(丁海峰)
Chin. Phys. B, 2024, 33 (**3**): 037501. DOI: 10.1088/1674-1056/ad188f

Magnonic band-pass and band-stop filters with structurally modulated waveguides

Lai-He Feng(冯来和), Mang-Yuan Ma(马莽原), Zhi-Hua Liu(刘智华), Kai-Le Xie(解凯乐), and Fu-Sheng Ma(马付胜)
Chin. Phys. B, 2023, 32 (**6**): 067503. DOI: 10.1088/1674-1056/ac8afb

Gate-voltage control of alternating-current-driven skyrmion propagation in ferromagnetic nanotrack devices

Xin-Yi Cai(蔡心怡), Zhi-Hua Chen(陈志华), Hang-Xiao Yang(杨航霄), Xin-Yan He(何鑫岩), Zhen-Zhen Chen(陈珍珍), Ming-Min Zhu(朱明敏), Yang Qiu(邱阳), Guo-Liang Yu(郁国良), and Hao-Miao Zhou(周浩淼)
Chin. Phys. B, 2023, 32 (**6**): 067502. DOI: 10.1088/1674-1056/acb420

Micromagnetic study of magnetization reversal in inhomogeneous permanent magnets

Zhi Yang(杨质), Yuanyuan Chen(陈源源), Weiqiang Liu(刘卫强), Yuqing Li(李玉卿), Liying Cong(丛利颖), Qiong Wu(吴琼), Hongguo Zhang(张红国), Qingmei Lu(路清梅), Dongtao Zhang(张东涛), and Ming Yue(岳明)
Chin. Phys. B, 2023, 32 (**4**): 047504. DOI: 10.1088/1674-1056/ac9359

Influence of Dzyaloshinskii-Moriya interaction on the magnetic vortex reversal in an off-centered nanocontact geometry

Hua-Nan Li(李化南), Tong-Xin Xue(薛彤鑫), Lei Chen(陈磊), Ying-Rui Sui(隋瑛瑞), and Mao-Bin Wei(魏茂彬)†
Chin. Phys. B, 2022, 31 (**9**): 097501. DOI: 10.1088/1674-1056/ac4cbd

---

Consistency between domain wall oscillation modes and spin wave modes in nanostrips

Xinwei Dong(董新伟)[†] and Zhenjiang Wu(吴振江)

Department of Physics and Institute of Theoretical Physics and Astrophysics, Xiamen University, Xiamen 361005, *China*

(Received 17 November 2023; revised manuscript received 29 January 2024; accepted manuscript online 19 February 2024)

Investigations on domain wall (DW) and spin wave (SW) modes in a series of nanostrips with different widths and thicknesses have been carried out using micromagnetic simulation. The simulation results show that the frequencies of SW modes and the corresponding DW modes are consistent with each other if they have the same node number along the width direction. This consistency is more pronounced in wide and thin nanostrips, favoring the DW motion driven by SWs. Further analysis of the moving behavior of a DW driven by SWs is also carried out. The average DW speed can reach a larger value of $\sim$ 140 m/s under two different SW sources. We argue that this study is very meaningful for the potential application of DW motion driven by SWs.

Keywords: micromagnetic simulation, domain wall, spin wave

PACS: 75.78.–n, 75.60.Ch, 75.78.Cd **DOI:** 10.1088/1674-1056/ad2a6b

1. Introduction

Recently, the controllable DW motions in ferromagnetic nanostrips have attracted increasing attention; firstly, due to their potential and practical applications in next-generation magnetic logic and memory devices,[1,2] and secondly, due to the emergence of considerable driving forces. To date, the controllable motions of DWs in nanostrips can not only be achieved by traditional driving forces, such as an external magnetic field[3–7] and a spin-polarized current,[8–11] but can also be obtained by alternative driving forces, such as an electric field,[12] SWs,[13–23] temperature gradients,[24–31] and polarized laser pulses.[32–36] Among them, the SW is recognized as one of the most potential driving forces due to its low energy dissipation and ultrafast velocity. When it is SW-driven, a 180° Néel DW (head-to-head) may move in either the same direction (mainly for the high-f SWs) or the opposite direction (for the low-f SWs) to that of SW propagation. For simplicity, these two distinguished DW-motion modes are classified into type-I (i.e., in the low-f range) and type-II modes (i.e., mainly in the high-f range), respectively. With regard to the underlying mechanisms, the angular momentum transfer from the SW to the DW is responsible for type-I DW-motion mode, whereas the linear angular momentum transfer is responsible for type-II mode.[17,37–39] Furthermore, it is worth noting that the DW motion is rather sensitive to the SW frequency ($f_{\rm SW}$). The corresponding $f_{\rm SW}$-dependent velocity curve, similar to the resonance spectra of the DW, also exhibits multi-peak characteristics, and their peaks are all consistent with each other. This may seem to imply the existence of some linkage between DW and SW modes. It is well known that the normal resonance modes of the DW in a nanostrip have been well studied,[19,40–42] as has the investigation of SW modes.[43–45] However, their relationship has not been reported yet. Additionally, it is worth mentioning that the investigation of the propagation of SWs inside a nano-sized DW has also attracted considerable attention.[46–48]

Based on this thinking, in this study, we carried out investigations on the relationship between DW and SW modes in a series of nanostrips. From the simulation results, one can observe the consistency between the frequencies of SW modes ($f_{{\rm SW},m}$) and the corresponding DW modes ($f_{{\rm DW},n}$) if they have the same node number along the width direction (i.e., $m = n$). This good consistency (occurring in wide and thin nanostrips) benefits the DW motion driven by SWs. Following this, we then carried out investigations on the moving behavior of DWs driven by SWs in a $3005\times80\times5$ nm^3 nanostrip.

2. Material and methods

In this study, the nanostrip size is set as 6 μm in length and 5 nm in thickness (t), and the width (w) is set in a wide range from 50 nm to 110 nm. In the simulations, the mesh cell size is selected as $2.5\times2.5\times5$ nm^3 and standard material parameter values of permalloy (Py) are used: the saturation magnetization $M_{\rm s} = 800\times10^3$ A/m, the exchange stiffness constant $A_{\rm ex} = 1.3\times10^{-11}$ J/m and the anisotropy constant $K = 0$. The Gilbert damping constant α is usually set as 0.01, but it is set in a wide range from 0.01 to 1 at the end of the nanostrip (with a length of 1500 nm) to absorb the SWs reflected by the end of the nanostrip. We used Mumax[3] to solve the Landau–Lifshitz–Gilbert (LLG) equation.[49]

One head-to-head DW (HHDW) was placed at the center of the nanostrip, as shown in Fig. 1(a). To excite the DW os-

[†]Corresponding author. E-mail: dongxw@xmu.edu.cn

© 2024 Chinese Physical Society and IOP Publishing Ltd

cillation, a field of H_z (0.001 T, with a time duration of 500 ps) was locally applied on the DW. Furthermore, for better excitation of high-f SWs in the nanostrip without a DW, a narrow Y-oriented domain (with magnetization oriented on the y-axis, as shown in Fig. 1(b)) at the end of a 3-μm-long nanostrip was deliberately set as the SW source instead of exciting the SWs by applying a sine function field along the y-axis.[45] The SWs will be generated from the relaxation of the Y-oriented domain to its equilibrium state (i.e., the X-oriented domain). The SW modes were obtained by the dispersion curves of the SWs, which were achieved by resolving fast Fourier transformation (FFT) of M_z in the 2 μm-long region near the SW source. With regard to the DW motion driven by SWs, a sine function of a field with a certain frequency was applied along the y-axis in a narrow area (∼ 5 nm wide) near the DW, which was placed at the center of the nanostrip, as shown in Fig. 1(a).

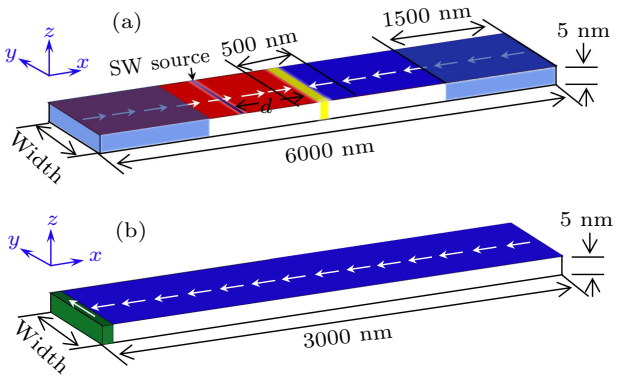


Fig. 1. (a) A schematic view of the model system for DW modes. One head-to-head DW was initially placed at the center of the nanostrip (yellow area). The area between the two black lines in the center of the nanostrip is the FFT area. The gray area (1500 nm long) at the end of the nanostrip, with a wide range of α from 0.01 to 1, is set to avoid the reflection of SWs. The white arrows represent the magnetization directions of domains. The sine function of a field with a certain frequency is applied along the y-axis in the purple area (with a distance d of DW), acting as the SW source to drive DW motion. (b) A schematic view of the model system for SW modes. The green area (5 nm wide) at the end of the nanostrip is set as the Y-oriented domain, serving as the SW source.

3. Results and discussion

We first investigated the DW resonance modes in an 80-nm-wide nanostrip. Both the FFT data and the DW modes were achieved by resolving FFT of M_z around the DW area (with a length of 0.5 μm, as shown in Fig. 1(a)). Figure 2 shows the FFT data and FFT power distributions of DW modes corresponding to the relevant FFT peaks (shown as the inserted figures). After a short-lived and local field of H_z applied to the DW area, resonance oscillations of the DW can separately or simultaneously occur in the DW center, at the DW boundaries and even in the adjacent area to the DW, forming edge modes, boundary modes, center modes, standing-wave modes and their mixed modes in a wide frequency range. Moreover, these oscillations may be out of phase or in phase with each other in the same area or among different areas (see the inserted figures in Fig. 2(b)).

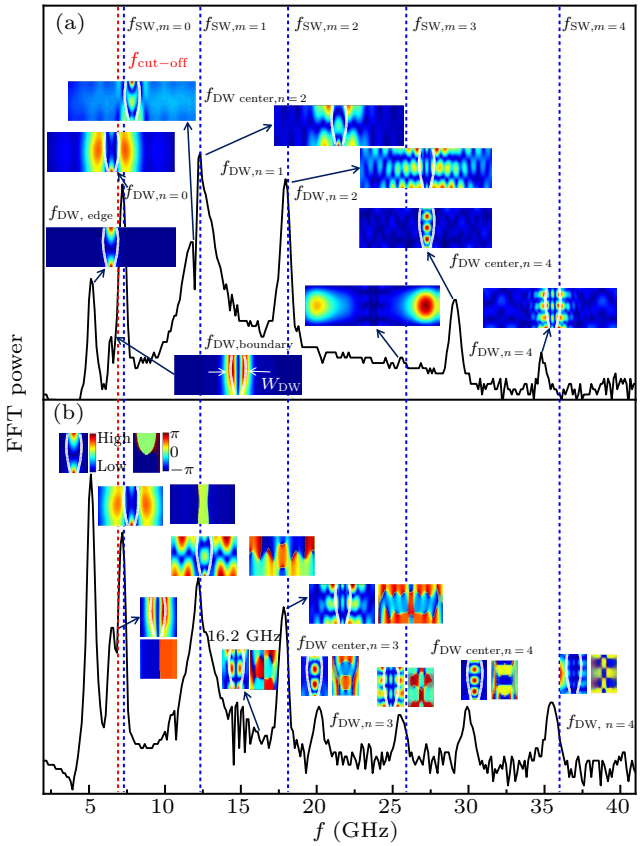


Fig. 2. FFT data of $M_z(t)$ around the DW area with a length of (a) 0.5 μm and (b) 0.2 μm on the x-axis. The FFT-peak-related spatial distributions of the FFT power (DW modes) are shown as insets in both (a) and (b), respectively. Spatial distributions of the FFT phase angle corresponding to the DW modes are only observable in (b), i.e., on the right or downside of the figures of FFT power distribution of the DW modes. White lines on the FFT power distribution of DW modes represent the DW width. The distance between two white arrows in the DW boundary mode is defined as the DW width. The values of $f_{cut-off}$ (dashed red line) and $f_{SW,m}$ (dashed blue lines) in the 80-nm-wide nanostrip, are 6.9 GHz and 7.3 GHz, 12.3 GHz, 18.1 GHz, 25.9 GHz, 36.0 GHz for $m = 0$, 1, 2, 3, 4, respectively.

Figure 2 also presents the $f_{SW,m}$, in which m means the node number of the SW along the y-axis, achieved by the dispersion curves of SWs in the 80-nm-wide nanostrip without the DW (see the dashed blue lines). The cut-off frequency of the SW ($f_{cut-off}$, see the dashed red lines) is slightly smaller than $f_{SW,m=0}$ (7.3 GHz), and can be confirmed as 6.9 GHz by the abrupt change in DW velocity in the following section. One can also easily see that the frequencies of the two DW modes are below $f_{cut-off}$, i.e., the single-region oscillation, which occurs at the lateral edge of the nanostrip ($f_{DW,edge}$ = 5.1 GHz) and at DW boundaries ($f_{DW,boundary}$ = 6.5 GHz). However, no SWs are emitted in such DW oscillations (see the inserted figures in Fig. 2(a)). It is understandable that the propagation of SWs with frequencies below $f_{cut-off}$ is prohibited. Above $f_{cut-off}$, the DW oscillations are all followed by the emission of SWs. Interestingly, if we define the frequencies of the DW modes (whose DW center and DW boundary

oscillations have the same node number of n, besides the case of $n = 1$) as $f_{\mathrm{DW},n}$, one can easily find that $f_{\mathrm{SW},m}$, to some extent, roughly equals $f_{\mathrm{DW},n}$ when $m = n$. For example, at $f_{\mathrm{DW},n=0} = 7.2$ GHz, an obvious wide-area oscillation with zero node (note that the oscillation mainly occurs at the adjacent area to the DW) is followed by the emission of an SW with zero node, whereas the SW mode with no node can be observed at $f_{\mathrm{SW},m=0} = 7.3$ GHz. A similar situation can also be found at $f_{\mathrm{DW},n=1} = 12.2$ GHz, and the emission of one-node SW can be clearly seen. Numerically, $f_{\mathrm{DW},n=1}$ is consistent with $f_{\mathrm{SW},m=1}$ (12.3 GHz). The same consistency can also be found at $f_{\mathrm{DW},n=2} = 17.8$ GHz; the related DW boundary and DW center oscillation both have two nodes and the excited SW also has two nodes, whereas the two-node SW comes out at $f_{\mathrm{SW},m=2} = 18.1$ GHz. With regard to the DW mode at 11.7 GHz, although the whole-DW-area oscillation is observable, the oscillation at the DW boundary is much weaker compared to the oscillation in the DW center. Furthermore, the DW center oscillation has two nodes, while one node is observable in the induced SW. Thus, it should be classified as the DW center oscillation mode.

However, the consistency between DW and SW modes becomes complicated in the high-f range from 26 GHz to 36 GHz. The three-node DW mode is missing, and the three-node SW can not only be induced by the DW center oscillation with four nodes ($f_{\mathrm{DW\ center},n=4} = 29.1$ GHz), but can also be produced by the whole-DW-area oscillation with four nodes ($f_{\mathrm{DW},n=4} = 34.8$ GHz). After careful observation of the four-node DW mode, the four-node SW is actually excited at DW boundaries, but it turns into a three-node SW quickly after a short distance propagation. This means that the high-f multi-nodal SWs ($m \geq 3$) can only be locally induced in the adjacent area to the DW by the DW oscillations. This can also be proved by the DW oscillation mode at ~ 25.6 GHz (see Fig. 2(a)) (which will be confirmed as $f_{\mathrm{DW},n=3}$ in the following section), although no obvious FFT peak is observable at ~ 25.6 GHz. As expected, the three-node DW oscillation mode is very weak, and so is the three-node SW induced by the DW oscillation. Their oscillation amplitudes are even smaller than that of the zero-node SW. Thus, among these DW modes, the three-node DW modes are negligible.

For further clarification, we carried out investigations on the excitation efficiency and attenuation length of SWs in the 80-nm-wide nanostrip. Figure 3 shows that the excitation efficiency and attenuation length of SWs are both highly dependent on f_{SW}.[16] They both have an abrupt increase in the low-f range and then decrease with f_{SW} after a peak. The maximum excitation efficiency appears around $f_{\mathrm{DW},n=0}$, while the attenuation length has an abrupt increment in a wider f-range from $f_{\mathrm{cut-off}}$ to $f_{\mathrm{DW},n=1}$. Furthermore, the excitation efficiency decreases abruptly after the peak, but the attenuation length decreases slowly after a wide and flat peak in a f-range from $f_{\mathrm{DW},n=1}$ to $f_{\mathrm{DW},n=2}$. Thus, due to the low excitation efficiency of the high-f SWs, the high-f SWs are much harder to generate in comparison to the low-f SWs. Even though the high-f SWs can be excited, they are very weak and only exist locally near the DW.

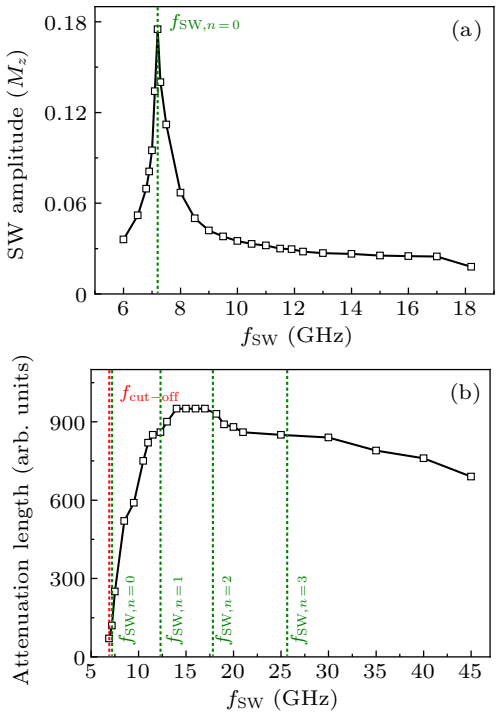


Fig. 3. The f_{SW}-dependence of the excitation efficiency (a) and attenuation length of SWs (b) in the 80-nm-wide nanostrip. The values of $f_{\mathrm{cut-off}}$ (dashed red line) and $f_{\mathrm{DW},n}$ (dashed green lines) in the 80-nm-wide nanostrip are 6.9 GHz and 7.2 GHz, 12.2 GHz, 17.8 GHz, 25.6 GHz for $n = 0$, 1, 2, 3, respectively.

Based on this analysis, we recalculated the FFT data and the DW oscillation modes by resolving FFT of M_z around the DW in a much narrower length (about 0.2 μm): good consistency between the DW and SW modes in the high-f range was finally achieved. As shown in Fig. 2(b), $f_{\mathrm{DW},n=3}$ (25.6 GHz) and $f_{\mathrm{DW},n=4}$ (35.5 GHz) are roughly consistent with their counterparts $f_{\mathrm{SW},m=3}$ (25.9 GHz) and $f_{\mathrm{SW},m=4}$ (36.0 GHz), respectively. It is worth mentioning that the value of $f_{\mathrm{DW},n}$ gets much smaller than that of $f_{\mathrm{SW},m}$ with the increasing node number (note that $m = n$). The fact that it is much easier to form a multi-nodal DW mode than an SW mode may be ascribed to the inhomogeneous distributions of an effective field in the DW, induced by its inhomogeneous equilibrium magnetization configuration.[42] The strip's lateral edges with a large effective field gradient can favor the confinement of the SW, resulting in easy formation of the localized edge modes. Conversely, the increasing frequency gap between the multi-nodal DW mode and the corresponding SW mode does not benefit the excitation of DW resonance oscillation, which plays a vital role in the DW driving process, and finally leads to the reduction of the DW motion speed. Furthermore, the DW center

oscillations with three nodes ($f_{\mathrm{DW\ center},n=3} = 20.2$ GHz) and four nodes ($f_{\mathrm{DW\ center},n=4} = 29.9$ GHz) are also observable, respectively. Also, an anti-symmetric DW oscillation mode at 16.2 GHz (a very tiny FFT peak) can be seen. Its oscillation mainly locates on both sides of the DW center line at $x = 0$ and is anti-symmetrical with respect to the DW central line, as shown in the inset of Fig. 2(b). These anti-symmetrical DW modes are more commonly seen in thick nanostrips.

It is well known that $f_{\mathrm{SW},m}$ in nanostrips will decrease with the increment of w.[45] As shown in Figs. 4(a) and 4(b), for the 5- and 10-nm-thick nanostrips, both $f_{\mathrm{SW},m}$ and $f_{\mathrm{DW},n}$ indeed decrease with increasing w, and become increasingly concentrated in the low-f range. Furthermore, their consistency is maintained well in these two series nanostrips. However, $f_{\mathrm{DW,edge}}$ behaves very uniquely. In the w-range from 110 nm to 60 nm, being the DW mode with the lowest frequency, $f_{\mathrm{DW,edge}}$ decreases slowly with the decrease in w, similar to $f_{\mathrm{DW},n=0}$. However, with a further decrease in w, $f_{\mathrm{DW,edge}}$ gets an abnormal increment at $w = 50$ nm, reaching up to 8.3 GHz (slightly larger than $f_{\mathrm{DW,boundary}}$, 7.9 GHz). When $w < 40$ nm, $f_{\mathrm{DW,edge}}$ gets a huge increment and is even twice the size of $f_{\mathrm{DW},m=0}$ at $w = 20$ nm (see Fig. 4(a)). With regard to the reason for this, we argue that it should be attributed to the smaller reduction of the edge DW mode area with the decrease in w (especially when $w < 40$ nm), compared to the other DW modes. For simplicity, we defined the DW width W_{DW} as the distance between two DW boundaries in the DW boundary mode along $y = 0$ (see Fig. 2(a)). We also defined the width of DW edge mode, $W_{\mathrm{DW,edge}}$, as the width of the oscillation area along the lateral edge of the nanostrip with a wider DW width. As shown in the inset of Fig. 4(a), $W_{\mathrm{DW,edge}}$ goes down more slowly than W_{DW} with the decrease in w. At $w = 20$ nm, $W_{\mathrm{DW,edge}}$ almost equals W_{DW}. Note that the narrower the nanostrip, the greater the amount of energy needed to induce a DW oscillation, especially in the almost whole DW area. The corresponding DW resonance frequency is going to be very high.

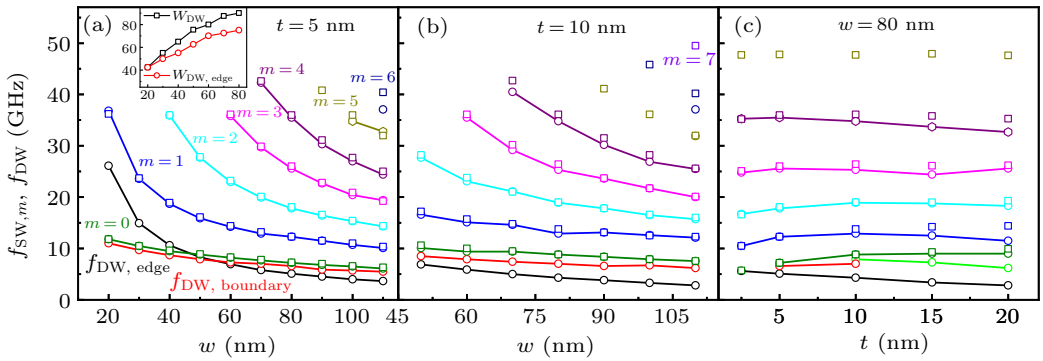


Fig. 4. The w-dependence of both $f_{\mathrm{SW},m}$ (square) and f_{DW} (circle) for (a) 5-nm-thick nanostrips and (b) 10-nm-thick nanostrips. The t-dependence of both $f_{\mathrm{SW},m}$ and f_{DW} for 80-nm-wide nanostrips. The inset values of m represent the node numbers of SW modes.

In Fig. 4(c), one can also observe the t-dependence of $f_{\mathrm{SW},m}$ in the 80-nm-wide nanostrips. In detail, the $f_{\mathrm{SW},m}$ in the low-f range ($m \leq 2$) increase with increasing t, while the high-f $f_{\mathrm{SW},m}$ are nearly saturated after $t = 5$ nm. Furthermore, the good consistency between $f_{\mathrm{SW},m}$ and $f_{\mathrm{DW},n}$ is only observable when $t \leq 10$ nm. Meanwhile, the DW modes below $f_{\mathrm{cut-off}}$ exhibit a strong thickness dependence. Some DW modes only exist in a narrow t-range, e.g., the DW boundary mode is only observable in the t-range from 5 nm to 10 nm, and the mixed mode of the DW edge and the DW boundary mode can be seen in the t-range from 10 nm to 20 nm. Interestingly, the DW edge mode and DW boundary mode both exhibit different thickness dependence, decreasing with the increment of t. Specifically, with the increment of t, the DW modes become more complicated. The possible reason for this may be the asynchronism of DW oscillation in the different layers when t reaches a certain value (around 10 nm), which definitely does not favor the DW motion. The underlying mechanism needs to be further investigated. Consequently, we argue that the wider and thinner the nanostrip, the easier it is to obtain high SW excitation efficiency and the easier it is to achieve fast DW motion driven by SWs.

We then investigated the moving behavior of DWs driven by the propagating SWs in the $3005\times80\times5$ nm^3 nanostrip. The distance (d) between the SW source and the DW was first set as a small value of 500 nm. At first glance, an abrupt decrement of the DW moving speed (which refers to the average speed of the DW in a time duration of 20 ns) from 34 m/s to 1.5 m/s at 6.9 GHz is observable, as shown in Fig. 5(a). Thus, the value of $f_{\mathrm{cut-off}}$ can be directly confirmed as 6.9 GHz. From the f_{SW}-velocity curve, two types of DW-motion modes can be easily distinguished. Type-I mode can be seen when f_{SW} lies in a narrow f-band above $f_{\mathrm{cut-off}}$ (i.e., 6.9 GHz $< f_{\mathrm{SW}} <$ 8.3 GHz), whereas the type-II mode is observable when f_{SW} is above 8.3 GHz. Furthermore, almost every DW speed peak, except the peak at 16.5 GHz, has the corresponding FFT resonance peak, and the high-f speed peak is much more consistent with the corresponding $f_{\mathrm{SW},m}$

than with $f_{\mathrm{DW},n}$ (e.g., the speed peak of 18.2 GHz is very near $f_{\mathrm{SW},m=2} = 18.1$ GHz). This further confirms that the high-f DW mode is hard to excite. With regard to the missing FFT peak at around 16.5 GHz, this should be ascribed to the peculiar and anti-symmetric oscillation of the DW in this frequency range (see the DW oscillation mode at 16.2 GHz in Fig. 2(b)). We assume that the anti-symmetric DW oscillation is hard to generate by applying a local field H_z on the DW. The unidirectional-propagation SWs possibly favor the generation of the anti-symmetric DW oscillation modes. Meanwhile, a tiny speed peak at $f_{\mathrm{DW},n=0}$ is also observable, although the main mode of DW motion at $f_{\mathrm{DW},n=0}$ is the type-I mode. Specifically, at $f_{\mathrm{DW},n=0}$, two DW motion modes coexist, while type-I takes a main role in the whole process. With increasing d, the dominant role of type-I mode is dramatically weakened, becomes negligible at $d = 750$ nm (Fig. 5(b) and the inset), and even vanishes at $d = 1500$ nm (Fig. 5(c) and the inset). Only a positive and small speed peak (representing type-II mode) can be found at $f_{\mathrm{DW},n=0}$. With regard to the reason for this, we assume that it should be ascribed to the extremely short attenuation length of the SWs in the f-range from 6.9 GHz to 8.3 GHz (Fig. 3(b)). Before propagating to the position of the DW, the SW is so attenuated that it cannot efficiently drive DW motion in type-I mode, but it can slightly induce DW oscillation and make the DW move in type-II mode. Further investigation of the underlying mechanism is needed. In addition, one can see that the maximum DW speed (51 m/s) appears at around $f_{\mathrm{SW},m=1}$, and the value of each speed peak roughly linearly decreases with increasing f_{SW}. The DW speed peak in the high-f range firstly vanishes with increasing d due to the low excitation efficiency of high-f SWs. Another possible reason may be the increasing frequency gap between the multi-nodal DW mode and the corresponding SW mode. Last but not least, the HHDW and tail-to-tail (TTDW) behave identically under the same SW.

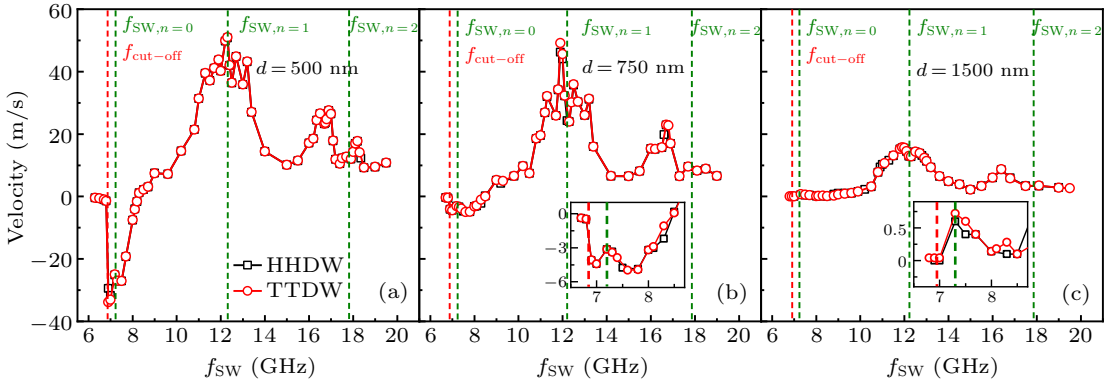


Fig. 5. The f_{SW}-dependence of the velocity of the head-to-head DW (square) and tail-to-tail DW (circle) in an 80-nm-wide nanostrip with a distance between the DW and SW source of (a) 500 nm, (b) 750 nm and (c) 1500 nm. The inset figures in (b) and (c) exhibit the detailed f_{SW}-velocity curves in the low-f range. The values of $f_{\mathrm{cut-off}}$ (dashed red line) and $f_{\mathrm{DW},n}$ (dashed green lines) in the 80-nm-wide nanostrip are 6.9 GHz and 7.2 GHz, 12.2 GHz, 17.8 GHz for $n = 0$, 1, 2, respectively.

Finally, if two DW-motion modes are simultaneously excited through two separate SW sources, the speed of the DW will achieve a much larger value. Taking the 80-nm-wide nanostrip as an example, SWs with frequencies of 7.2 GHz and 12.2 GHz were simultaneously excited. Two SW sources on each side of the DW have a distance of 500 nm, and the SW source with a frequency of 12.2 GHz is nearly close to the DW. Following the emission of two SWs, the average DW speed can reach a much larger value of $\sim$ 140 m/s.

4. Conclusions

In summary, we carried out investigations of DW and SW modes in a series of nanostrips with different w and t. One can easily observe the consistency between $f_{\mathrm{SW},m}$ and $f_{\mathrm{DW},n}$ when $m = n$. And the good consistency (occurring in wide and thin nanostrips) will favor the DW motion driven by SWs. Meanwhile, the f_{SW}-dependent DW speed curve shows two different DW-motion modes; type-I mode lies in a narrow-f band (i.e., 6.9 GHz $< f_{\mathrm{SW}} <$ 8.3 GHz), whereas type-II mode is in a wide-$f$band above $f_{\mathrm{cut-off}}$. Interestingly, two DW-motion modes coexist under the low-f SWs, and the type-I DW mode can only be observed near the SW source due to the short attenuation length of low-f SWs. Finally, the average DW speed can reach a larger value of $\sim$ 140 m/s under two different SW sources. We argue that this study is very meaningful for the potential application of DW motion driven by SWs.

Acknowledgements

Project supported by the Fundamental Research Funds for the Central Universities (Grant No. 20720210030) and the National Natural Science Foundation of China (Grant No. 11204255).

References

[1] Allwood D, Xiong G, Faulkner C C, Atkinson D, Petit D and Cowburn R P 2005 *Science* **309** 1688

[2] Parkin S S P, Hayashi M and Thomas L 2008 *Science* **320** 190
[3] Schryer N L and Walker L R 1974 *J. Appl. Phys.* **45** 5406
[4] Ono T, Miyajima H, Shigeto K, Mibu K, Hosoito N and Shinjo T 1999 *Science* **284** 468
[5] Beach G S D, Nistor C, Knutson C, Tsol M and Erskine J L 2005 *Nat. Mater.* **4** 741
[6] Omari K, Bradley R C, Broomhall T J, Hodges M P P, Rosamond M C, Linfield E H, Im M Y, Fischer P and Hayward T J 2015 *Appl. Phys. Lett.* **107** 222403
[7] Dong X W and Wang R F 2019 *J. Magn. Magn. Mater.* **473** 26
[8] Vernier N, Allwood D A, Atkinson D, Cooke M D and Cowburn R P 2004 *Europhys. Lett.* **65** 526
[9] Yamaguchi A, Ono T, Nasu S, Miyake K, Mibu K and Shinjo T 2004 *Phys. Rev. Lett.* **92** 077205
[10] Beach G S D, Knutson C, Nistor C, Tsoi M and Erskine J L 2006 *Phys. Rev. Lett.* **97** 057203
[11] Hayashi M, Thomas L, Rettner C, Moriya R, Bazaliy Y B and Parkin S S P 2007 *Phys. Rev. Lett.* **98** 037204
[12] Franke K J A, Van de Wiele B, Shirahata Y, Hämäläinen S J, Taniyama T and Dijken S V V 2015 *Phys. Rev. X* **5** 011010
[13] Han D S, Kim S K, Lee J Y, Hermsdoerfer S, Schiltheiss H, Leven B and Hillebrands B 2009 *Appl. Phys. Lett.* **94** 112502
[14] Seo S M, Lee H W, Kohno H and Lee K J 2011 *Appl. Phys. Lett.* **98** 012514
[15] Zhang S F, Mu C P, Zhu Q Y, Zheng Q, Liu X Y, Wang J B and Liu Q F 2014 *J. Appl. Phys.* **115** 013908
[16] Gao Z-C, Su Y, Weng L, Hu J and Park C 2019 *New J. Phys.* **21** 063014
[17] Yan P, Wang X S and Wang X R 2011 *Phys. Rev. Lett.* **107** 177207
[18] Kim J S, Stärk M, Kläui M, Yoon J, You C Y, Lopez-Diaz L and Martinez E 2012 *Phys. Rev. B.* **85** 174428
[19] Wang X G, Guo G H, Zhang G F, Nie Y Z and Xia Q L 2013 *J. Appl. Phys.* **113** 213904
[20] Covington M, Crawford T M and Parker G J 2002 *Phys. Rev. Lett.* **89** 237202
[21] Vlaminck V and Bailleul M 2008 *Science* **322** 410
[22] Choi S, Lee K S, Guslienko K Y and Kim S K 2007 *Phys. Rev. Lett.* **98** 087205
[23] Woo S, Delaney T and Beach G S D 2017 *Nat. Phys.* **13** 448
[24] Torrejon J, Malinowski G, Pelloux M, Weil R, Thiaville A, Curiale J, Lacour D, Montaigne F and Hehn M 2012 *Phys. Rev. Lett.* **109** 106601
[25] Jiang W J, Upadhyaya P and Fan Y B, *et al.* 2013 *Phys. Rev. Lett.* **110** 177202
[26] Wang X S and Wang X R 2014 *Phys. Rev. B* **90** 014414
[27] Tetienne J P, Hingant T, Kim J V, Herrera Diez L, Adam J P, Garcia K, Roch J F, Rohart S and Thiaville A 2014 *Science* **344** 1366
[28] Schlickeiser F, Ritzmann U, Hinzke D and Nowak U 2014 *Phys. Rev. Lett.* **113** 097201
[29] Selzer S, Atxitia U, Ritzmann U, Hinzke D and Nowak U 2016 *Phys. Rev. Lett.* **117** 107201
[30] Moretti S, Raposo V, Martinez E and Lopez-Diaz L 2017 *Phys. Rev. B* **95** 064419
[31] Yan Z, Chen Z, Qin M, Lu X, Gao X and Liu J 2018 *Phys. Rev. B* **97** 054308
[32] Stanciu C D, Hansteen F, Kimel A V, Kirilyuk A, Tsukamoto A, Itoh A and Rasing T 2007 *Phys. Rev. Lett.* **99** 047601
[33] Němec P, Rozkotová E and Tesařová N, *et al.* 2012 *Nat. Phys.* **8** 411
[34] Lambert C H, Mangin S and Varaprasad B S D C S, *et al.* 2014 *Science* **345** 1337
[35] Ramsay A J, Roy P E, Haigh J A, Otxoa R M, Irvine A C, Janda T, Campion R P, Gallagher B L and Wunderlich J 2015 *Phys. Rev. Lett.* **114** 067202
[36] Janda T, Roy P E and Otxoa R M, *et al.* 2017 *Nat. Commun.* **8** 15226
[37] Yan P, Kamra A, Cao Y and Bauer G E W 2013 *Phys. Rev. B* **88** 144413
[38] Yan P and Bauer G E W 2012 *Phys. Rev. Lett.* **109** 087202
[39] Yan P, Cao Y and Sinova J 2015 *Phys. Rev. B* **92** 100408
[40] Roy P E, Trypiniotis T and Barnes C H W 2010 *Phys. Rev. B* **82** 134411
[41] Metaxas P J, Albert M, Lequeux S, Cros V, Grollier J, Bortolotti P, Anane A and Fangohr H 2016 *Phys. Rev. B* **93** 054414
[42] Wang X G, Guo G H, Zhang G F, Nie Y Z, Xia Q L and Li Z X 2013 *J. Magn. Magn. Mater.* **332** 56
[43] Lee K S, Han D S and Kim S K 2009 *Phys. Rev. Lett.* **102** 127202
[44] Choi S, Lee K S, Guslienko K Y and Kim S K 2007 *Phys. Rev. Lett.* **98** 087205
[45] Bao D, and Dong X W 2021 *J. Magn. Magn. Mater.* **539** 168388
[46] Wagner K, Kákay A, Schultheiss K, Henschke A, Sebastian T and Schultheiss H 2016 *Nat. Nanotechnol.* **11** 432
[47] Henry Y, Stoeffler D, Kim J V and Bailleul M 2019 *Phys. Rev. B* **100** 024416
[48] Chang L J, Chen J L, Qu D R, Tsai L Z, Liu Y. F, Kao M Y, Liang J Z, Wu T S, Chuang T M, Yu H M and Lee S F 2020 *Nano Lett.* **20** 3140
[49] Vansteenkiste1 A, Leliaert J, Dvornik M, Helsen M, Garcia-Sanchez F and Van Waeyenberge B 2014 *AIP Adv.* **4** 107133